SUPPORTING INFORMATION

CYP2C19 and 3A4 dominate metabolic clearance and bioactivation of terbinafine based on computational and experimental approaches

Mary A. Davis[1], Dustyn A. Barnette[1], Noah R. Flynn[2], Anirudh S. Pidugu[3], S. Joshua Swamidass[2], Gunnar Boysen[4], Grover P. Miller*[1]

Table S1. Impact of reaction conditions on TBF-A decay in the absence of NADPH[a]

Isozyme		HLM	Control Supersomes	Recombinant Isozyme
CYP2C19	**Plateau (μM)**	2.44 ± 0.772	2.26 ± 2.11	3.86 ± 1.62
	Half-Life (μM)	12.2 ± 1.19	14.9 ± 2.88	13.7 ± 2.43
CYP3A4	**Plateau (μM)**	0.78 ± 1.44	2.58 ± 1.04	2.74 ± 1.76
	Half-Life (μM)	10.4 ± 2.11	17.2 ± 2.58	16.0 ± 4.05

[a]Depletion time course parameters for 50 μM TBF-A in the presence of protein preparation systems. Values for the plateau and half-life generated from the TBF-A depletion data as shown in **Fig. S2**. Standard deviations for constants are shown.

Table S2. Oxidative non-dealkylation steady-state kinetics and modeling predictions for CYP2C19[a]

Substrate	Metabolite	Kinetic equation[b]	Kinetic constants			Model output (position)[d]				
			V_{max}[c]	Hill Slope (n)	K_m or S_{50} (μM)	6*	3'	4'	5'	6'
terbinafine	dihydrodiol	Hill	0.32 ± 0.05	0.58 ± 0.08	110 ± 63	-	0.04	0.07	0.06	0.11
	hydroxyterbinafine	Hill	0.63 ± 0.02	1.41 ± 0.11	44.1 ± 2.9	0.72	-	-	-	-
desmethyl-terbinafine	dihydrodiol	Michaelis-Menten	0.077 ± 0.003	-	68.3 ± 9.5	-	0.06	0.09	0.09	0.14
	hydroxydesmethyl-terbinafine	Michaelis-Menten	0.028 ± 0.001	-	51.6 ± 7.4	0.75	-	-	-	-

[a]Standard deviations for constants are shown.
[b]Mechanism chosen was most statically preferred based on the extra sum-of-squares F test.
[c]Units are μV*sec due to the absence of authentic standards for quantitation.
[d]Refer to **Fig. S9** for positions targeted for oxidative metabolism. At position 6, there are three equivalent methyl groups attached to the carbon that shared a common terminal oxidation prediction value as shown.

Table S3. Oxidative non-dealkylation steady-state kinetics and modeling predictions for CYP3A4[a]

Substrate	Metabolite	Kinetic equation[b]	Kinetic constants			Model output (position)				
			V_{max}[c]	Hill Slope (n)	K_m or S_{50} (μM)	6*	3'	4'	5'	6'
terbinafine	dihydrodiol	Hill	0.44 ± 0.01	1.98 ± 0.32	17.6 ± 1.3	-	0.13	0.10	0.09	0.26
	hydroxyterbinafine	Hill	1.71 ± 0.06	1.30 ± 0.16	25.4 ± 2.3	0.07	-	-	-	-
desmethyl-terbinafine	dihydrodiol	Michaelis-Menten	0.0070 ± 0.0005	-	98 ± 19	-	0.16	0.11	0.11	0.29
	hydroxydesmethyl-terbinafine	Michaelis-Menten	0.00158 ± 0.00011	-	82 ± 20	0.08	-	-	-	-

[a]Standard deviations for constants are shown.
[b]Mechanism chosen was most statically preferred based on the extra sum-of-squares F test.
[c]Units are μV*sec due to the absence of authentic standards for quantitation.
[d]Refer to **Fig. S9** for positions targeted for oxidative metabolism. At position 6, there are three equivalent methyl groups attached to the carbon that shared a common terminal oxidation prediction value as shown.

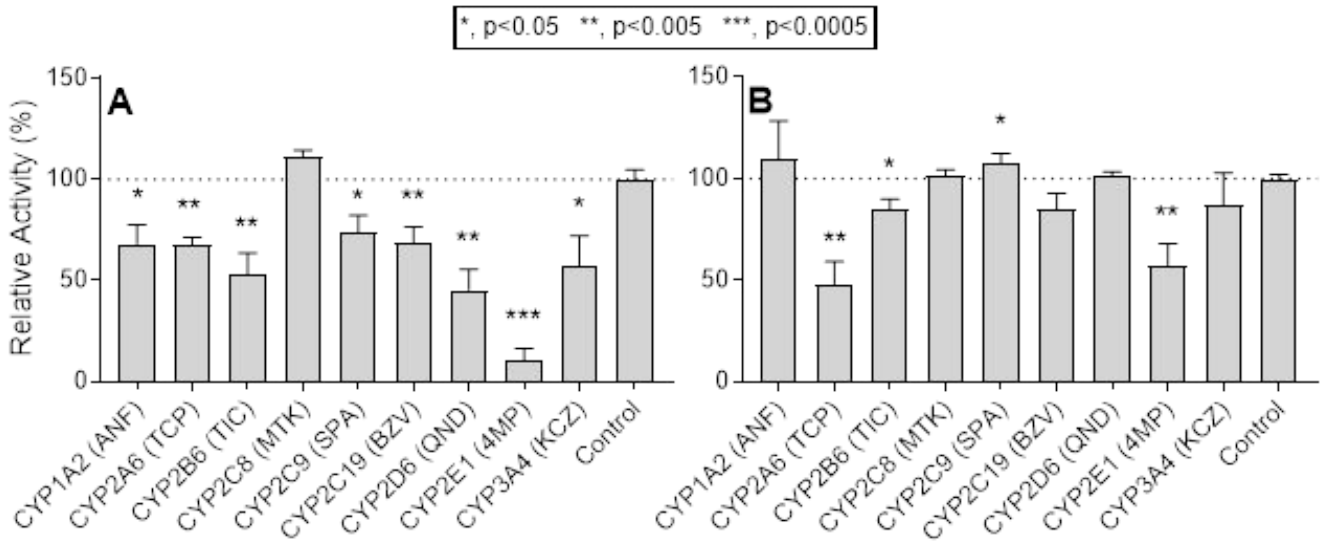

Fig. S1. Cytochrome P450 isozymes responsible for terbinafine oxidative non-dealkylations identified by inhibitor phenotyping. As described under Materials and Methods, terbinafine (500 μM) metabolism was blocked by P450-specific inhibitors in the formation of terbinafine dihydrodiols (**Panel A**) and hydroxyterbinafine (**Panel B**) (see **Figure 1** for structures). Error bars denote standard deviations. Inhibitors used are as follows: 16 μM α-naphthoflavone (ANF) for CYP1A2, 2 μM tranylcypromine (TCP) for CYP2A6, 3 μM ticlopidine (TIC) for CYP2B6, 16 μM montelukast (MTK) for CYP2C8, 10 μM sulfaphenazole (SPA) for CYP2C9, 16 μM (+)-N-3-benzylnirvanol (BZV) for CYP2C19, 2 μM quinidine (QND) for CYP2D6, 30 μM 4-methylpyrazole (4MP) for CYP2E1, and 1 μM ketoconazole (KCZ) for CYP3A4.

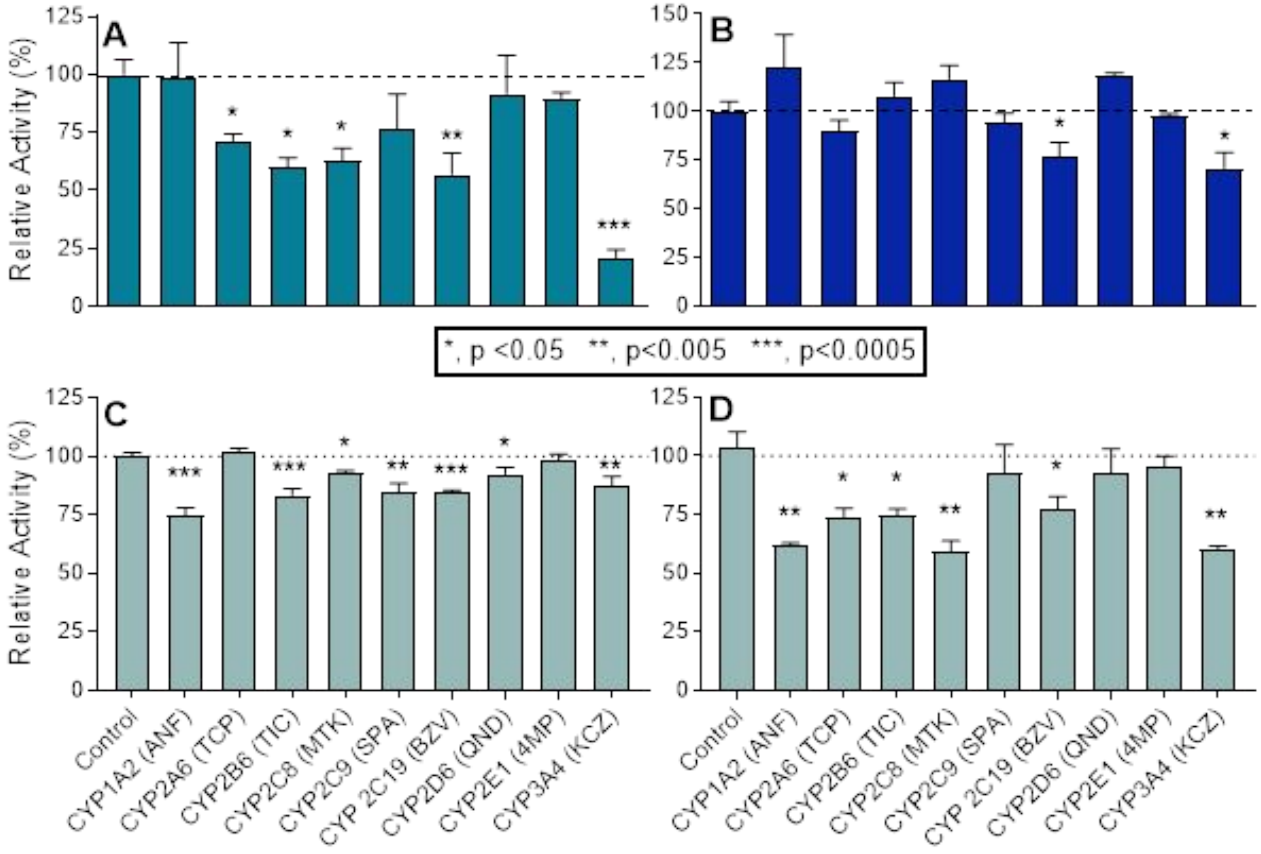

Fig. S2. Cytochrome P450 isozymes identified by inhibitor phenotyping of desmethyl-terbinafine metabolism. As described under Materials and Methods, desmethyl-terbinafine (200 μM) metabolism was blocked by P450-specific inhibitors in the formation of TBF-A (**Panel A**) from Step 2.2a, 1-naphthaldehyde (**Panel B**) from Step 2.2b, and the oxidative non-dealkylation metabolites, the dihydrodiols (**Panel C**) and hydroxyterbinafine (**Panel D**). Error bars denote standard deviations. All other potential metabolites for these reactions were not detected consistently or at all. Inhibitors used are as follows: 16 μM α-naphthoflavone (ANF) for CYP1A2, 2 μM tranylcypromine (TCP) for CYP2A6, 3 μM ticlopidine (TIC) for CYP2B6, 16 μM montelukast (MTK) for CYP2C8, 10 μM sulfaphenazole (SPA) for CYP2C9, 16 μM (+)-N-3-benzylnirvanol (BZV) for CYP2C19, 2 μM quinidine (QND) for CYP2D6, 30 μM 4-methylpyrazole (4MP) for CYP2E1, and 1 μM ketoconazole (KCZ) for CYP3A4.

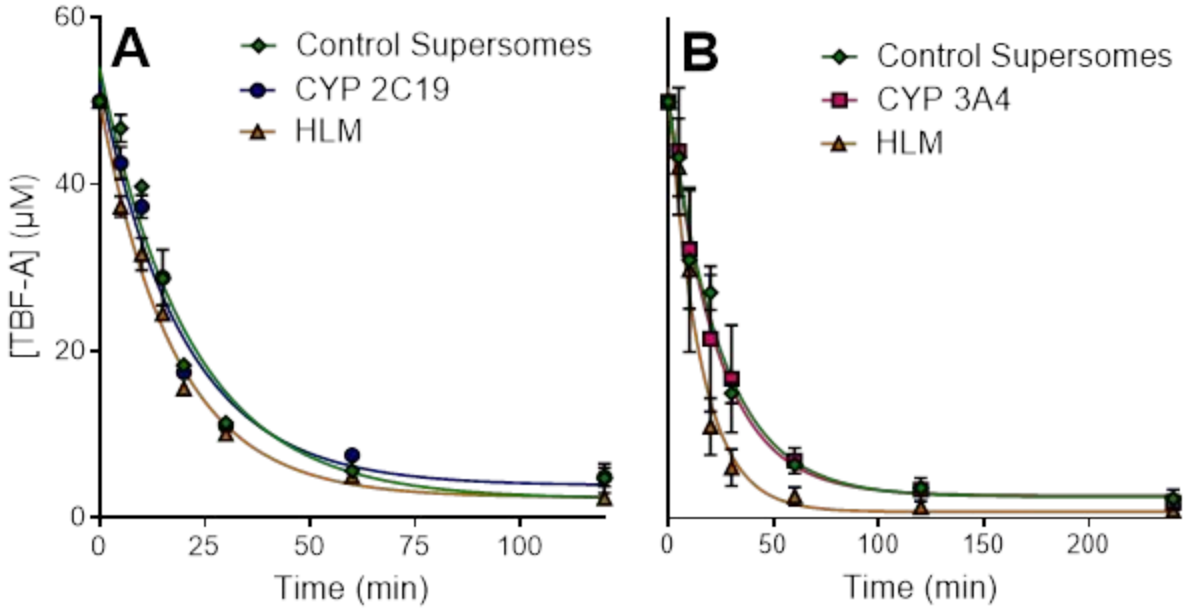

Fig. S3. TBF-A decayed under reaction conditions. Control experiments were conducted to further study decay of TBF-A under several enzymatic environments to confirm kinetic values. Decay of 50 µM TBF-A in control Supersomes, pooled human liver microsomes (HLM), and recombinant CYP2C19 (**Panel A**) or CYP3A4 (**Panel B**) was studied. Error bars denote standard deviations. Reactions were conducted and quenched at each time point to discern rate of TBF-A decay as described in Materials and Methods.

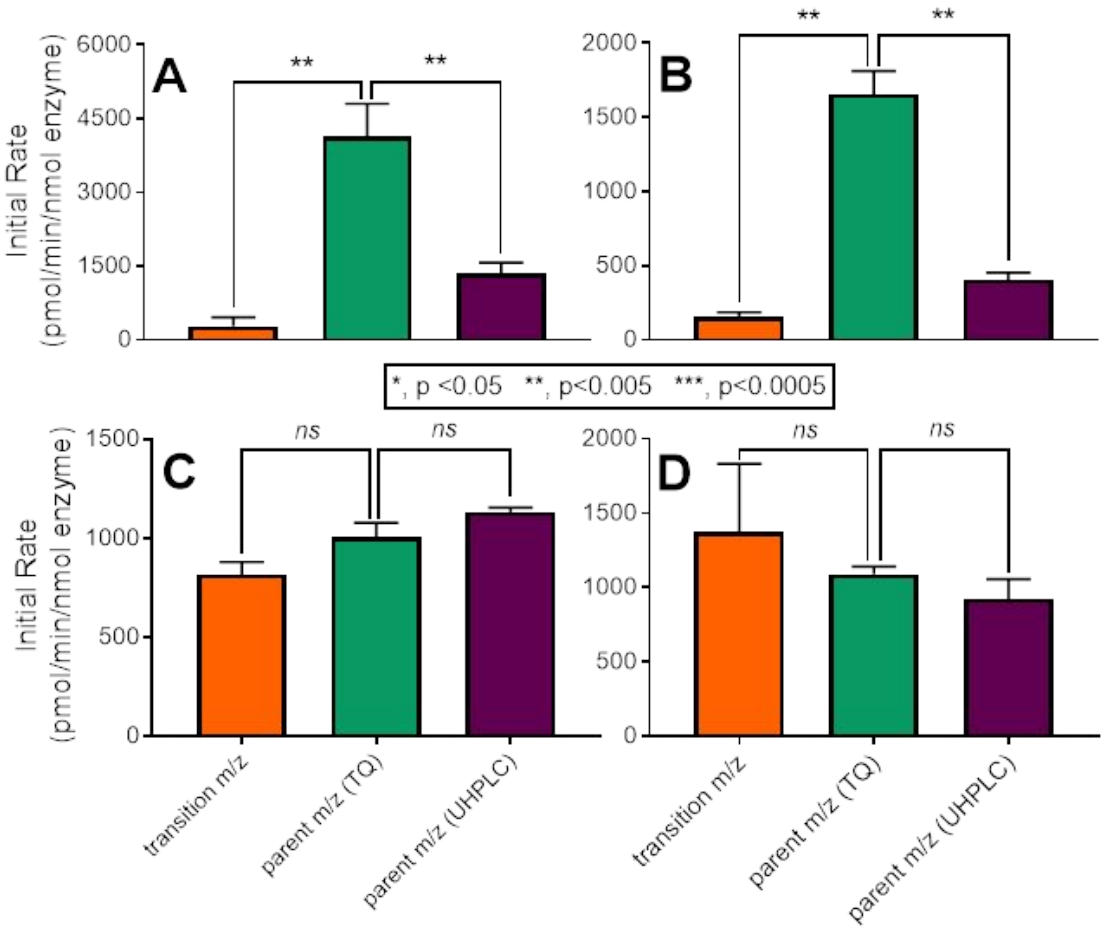

Fig. S4. MS response for dansylated TBF-A but not N-methyl-1-naphthyl methylamine varied among instruments. Results from UHPLC-MS/MS and UHPLC-MS analysis of recombinant P450 isozyme reactions using different instruments to assess differences seen between isozyme used, metabolite formed, and machine response. **Panels A and B** show initial rate of TBF-A formation (CYP2C19 and 3A4, respectively) from 500 μM measured using three detection methods: transition m/z via LC-MS/MS, parent m/z via LC-MS/MS (abbreviated as TQ), and parent m/z via UHPLC. **Panels C and D** (CYP2C19 and 3A4, respectively) show initial rate of the TBF-A co-metabolite, N-methyl-1-naphthyl methylamine, using the same detection methods. TBF-A initial rates vary significantly with each detection method, but N-methyl-1-naphthyl methylamine initial rates do not (denoted as '*ns*'), indicating their reliability as a measure of kinetics for the formation of both co-metabolites. Error bars denote standard deviations.

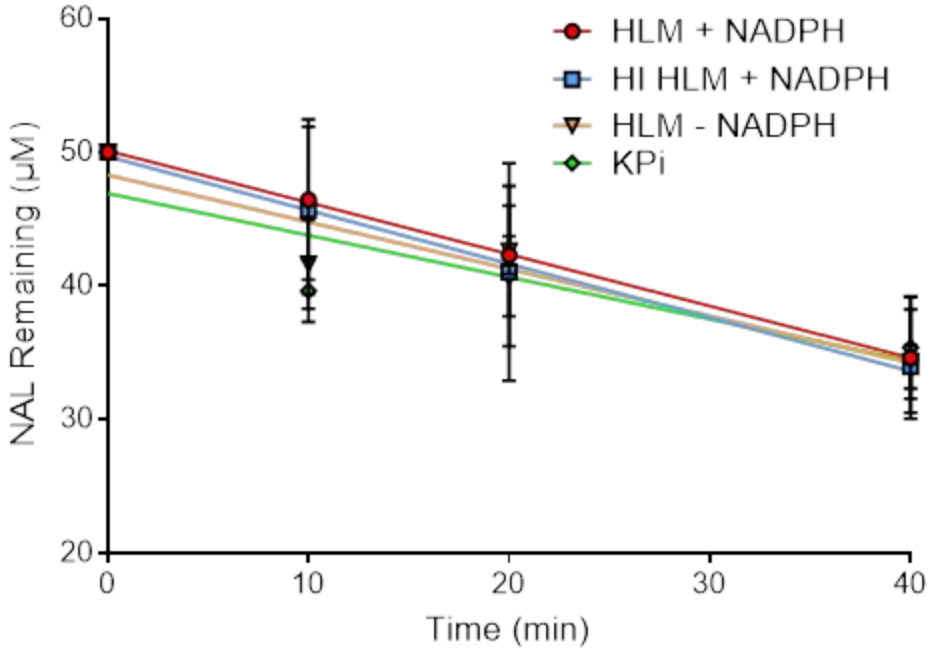

Fig. S5. 1-Naphthylaldehyde depletion was not impacted by human liver microsomal reaction conditions over time.-Our previous studies showed that 1-naphthaldehyde (NAL) decays under reaction conditions with human liver microsomes (HLM) as described for reactions in Materials and Methods. This experiment was conducted to determine whether presence of NADPH, human liver microsomes, or heat inactivation (HI) of microsomes contributed to 1-naphthaldehyde decay over a period of 40 min. Decay of 50 µM 1-naphthaldehyde was not significantly altered in active and heat-inactivated microsomes, phosphate buffer (KPi), with or without NADPH. Error bars denote standard deviations.

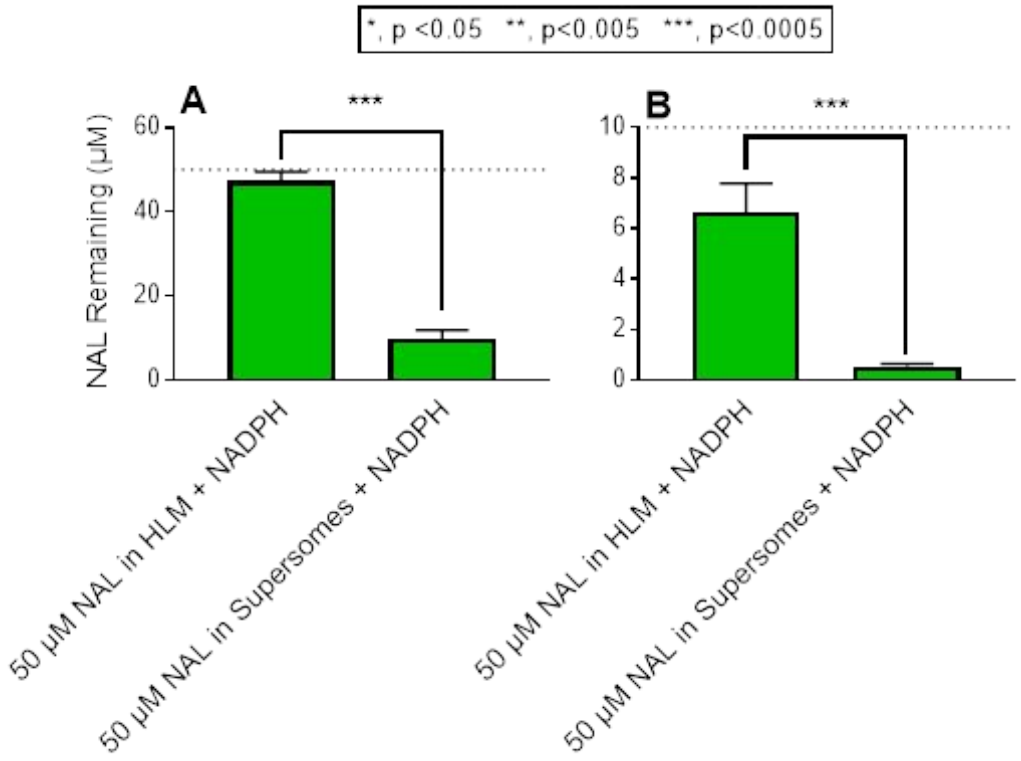

Fig. S6. In the presence of NADPH, Supersomes increased 1-napthaldehyde decay relative to microsomes. For comparative purposes, we measured 1-napthaldehyde (NAL) decay and its concentration-dependency for CYP2C19 and 3A4 Supersomes as well as human liver microsomes in the presence of NADPH as described for reactions in Materials and Methods. CYP2C19 and 3A4 were mixed at equivalent concentrations to form the "Supersome" mix used as a representative preparation. Studies were carried out over 30 min for 10 (**Panel A**) or 50 µM (**Panel B**) 1-naphthaldehyde decay in human liver microsomes and Supersomes. Error bars denote standard deviations.

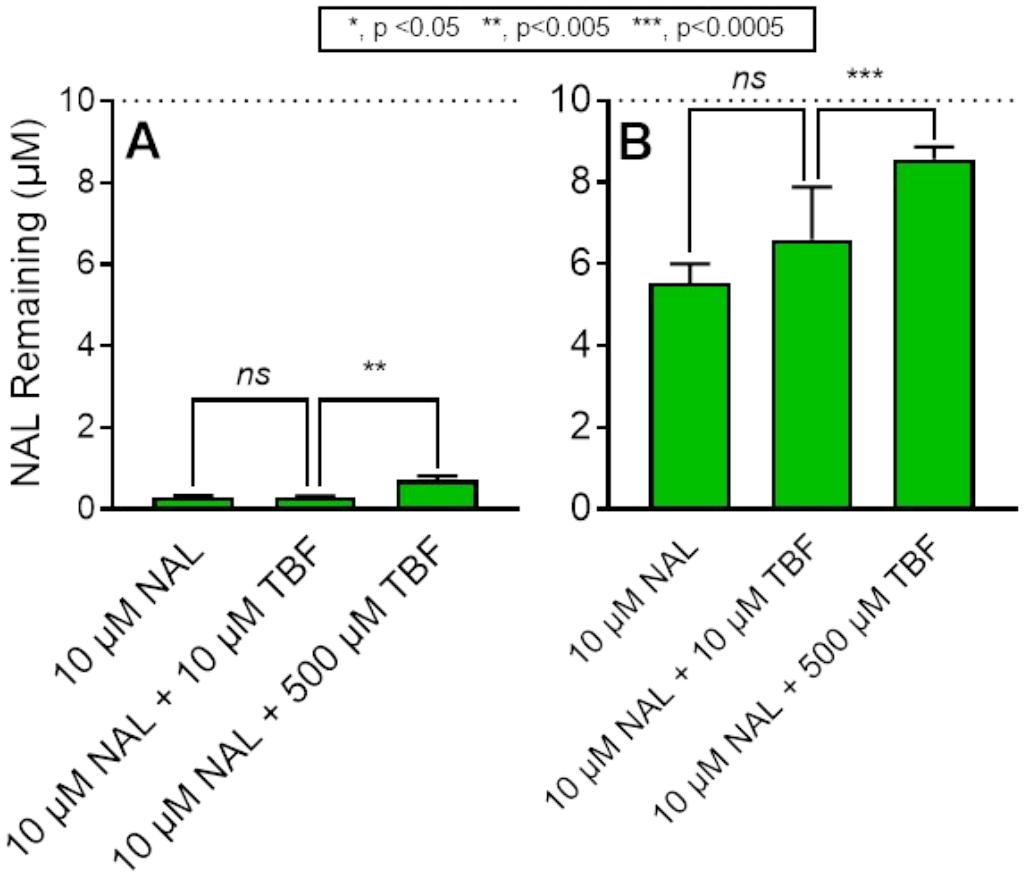

Fig. S7. Terbinafine at high levels blocked 1-napthaldehyde decay. Given 1-napthaldehyde (NAL) decay in Supersomes, we attempted to block any possible enzymatic reaction by adding either 10 μM or 500 μM terbinafine to a 10 μM 1-napthaldehyde reaction containing NAPDH. The data for CYP2C19 and 3A4 Supersomes are shown in **Panels A and B**, respectively. Error bars denote standard deviations. Reaction conditions and data analyses were carried out as described in Materials and Methods.

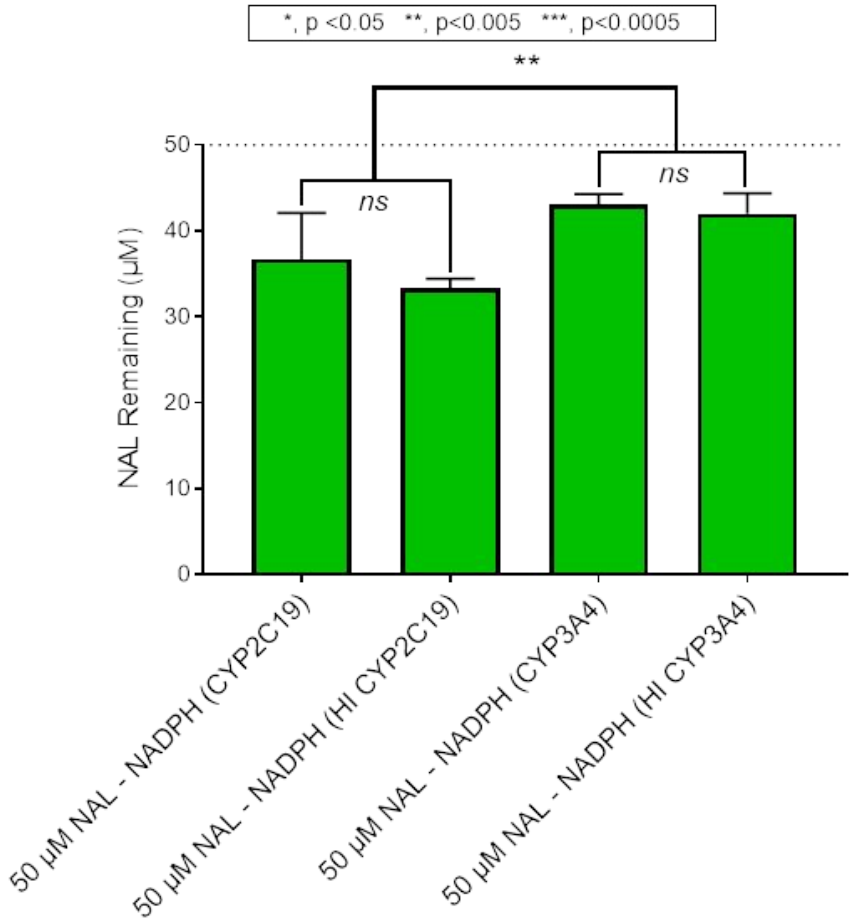

Fig. S8. Decay of 1-napthaldehyde in the presence of Supersomes was minimal in absence of NADPH. Incubation of 50 µM 1-naphthaldehyde (NAL) under reaction conditions for Supersomes, but in the absence of NADPH, led to marginal decrease in levels. There was no change in this effect when CYP2C19 and 3A4 were heat inactivated (HI) to denature the active enzymes. Error bars denote standard deviations. Reaction conditions and data analyses were carried out as described in Materials and Methods.

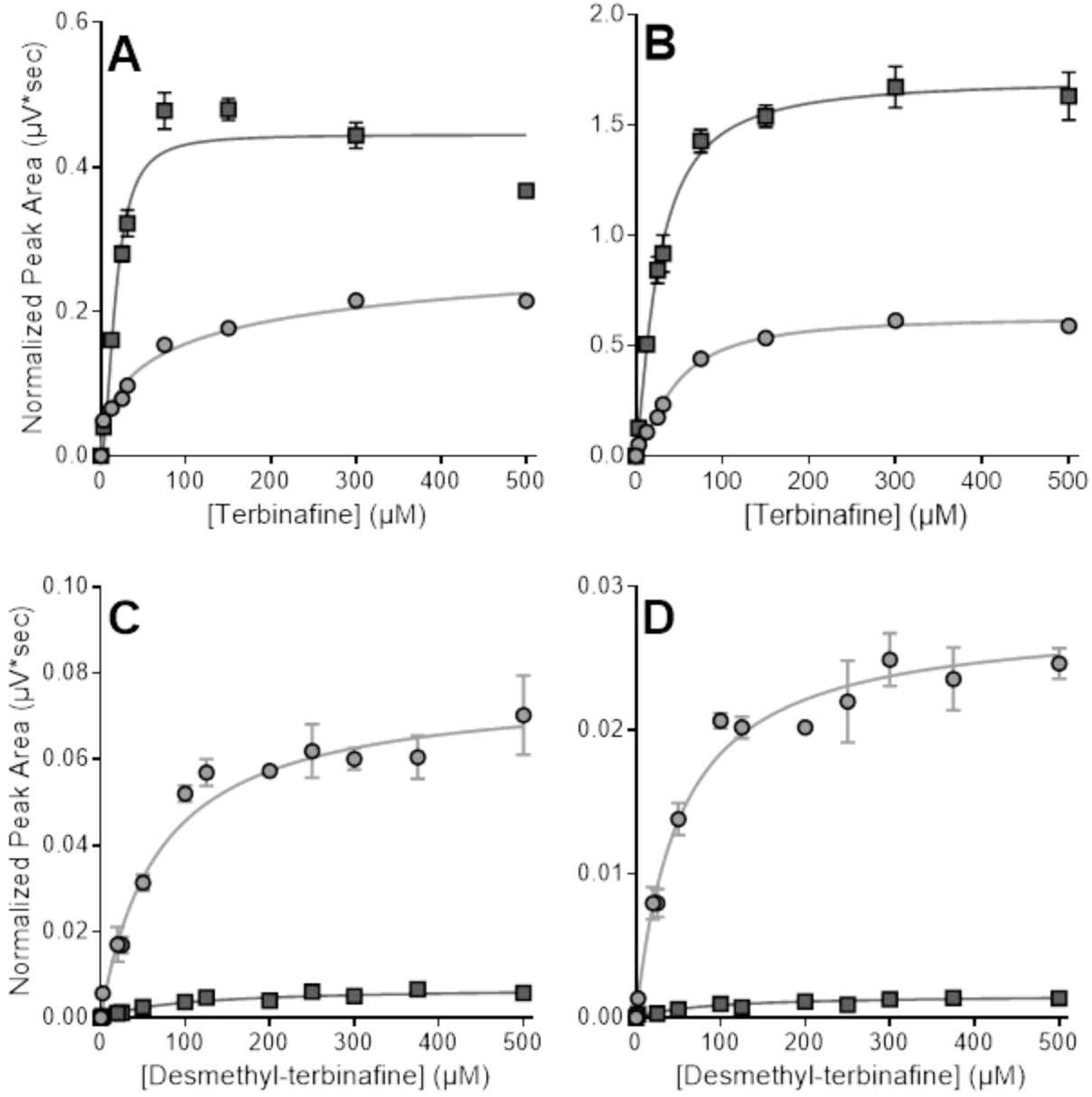

Fig. S9. CYP2C19 and 3A4 catalyzed oxidative non-dealkylations of terbinafine and desmethyl-terbinafine under steady-state conditions. Steady-state reactions yielded several metabolites from oxidative pathways not involving N-dealkylation. No quantitative standards for the products were available, so data was reported based on MS peak area. No labeling was used for detection of these metabolites. Terbinafine reactions yielded profiles for (**Panel A)** two isomers of terbinafine dihydrodiol (m/z 326) and (**Panel B**) hydroxyterbinafine (m/z 308). (**Panel C**) Desmethyl-terbinafine reactions yielded profiles for two isomers of desmethyl-terbinafine dihydrodiol (m/z 312) and (**Panel D**) hydroxydesmethyl-terbinafine (m/z 294) not shown in **Fig. 1**. Twelve experimental reactions were carried out for each substrate. Error bars denote standard deviations. Reaction conditions were carried out as described in Materials and Methods.

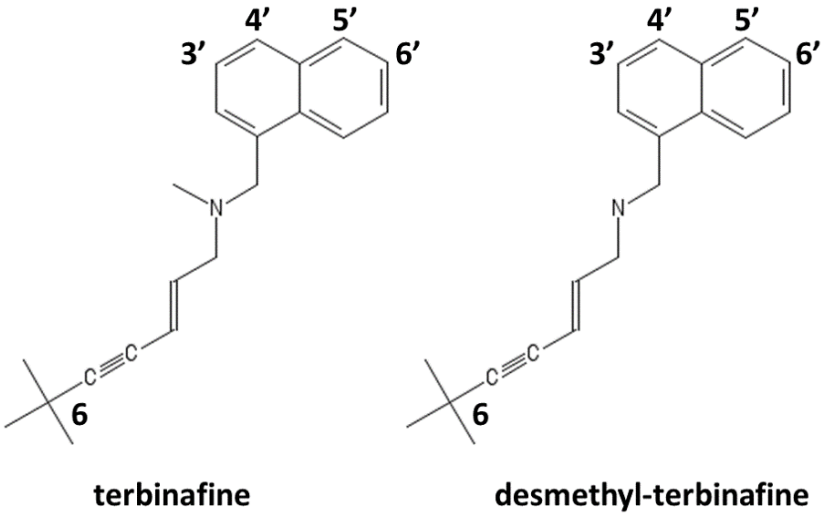

Fig. S10. Models predicted sites and likelihood for metabolism leading to dihydrodiols and terminally hydroxylated metabolites. The image denotes the sites of oxidative metabolism for terbinafine and desmethyl-terbinafine, which did not involve N-dealkylations. Actual predictions are summarized in **Tables S2** and **S3** for CYP2C19 and 3A4, respectively.